Long Unfolded Linkers Facilitate Membrane Protein Import Through the Nuclear Pore Complex

Anne C. Meinema *et al.*

Science **333**, 90 (2011);
DOI: 10.1126/science.1205741

Science (print ISSN 0036-8075; online ISSN 1095-9203) is published weekly, except the last week in December, by the American Association for the Advancement of Science, 1200 New York Avenue NW, Washington, DC 20005.

prominent accumulation of storage material of high electron density (Fig. 4B and fig. S4). In cells of patients or mice with various lysosomal storage disorders, secondary accumulation of lipids was observed (*21*). In SRD-12B cells, a variable number showed an accumulation of unesterified cholesterol and a moderate increase in staining intensity of the unusual lysophospholipid bis(monoacylglycero)phosphate (BMP). Both lipids colocalized partially with the lysosomal marker protein Lamp2 (Fig. 4C and fig. S5). These data indicate that partial deficiencies of lysosomal enzymes in mutagenized and selected SRD-12B cells are sufficient to alter lysosomal functions.

Here we have provided evidence that S1P-mediated cleavage of the α/β-subunit precursor is associated with the activation of GlcNAc-1-phosphotransferase, which is required for proper transport of lysosomal enzymes. The requirement of S1P for activation of the GlcNAc-1-phosphotransferase activity, combined with its established role in lipid metabolism, indicates the importance of S1P for lysosome biogenesis and function. This may have implications for diagnosis of individuals with genetically undefined mucolipidosis II–like phenotypes such as Pacman dysplasia (*22*). Moreover, these findings raise the question of beneficial use of S1P inhibitors to reduce the synthesis of cholesterol, low-density lipoprotein (LDL), and fatty acids in treating cardiovascular disorders or as an antiviral therapy (*23*–*25*) owing to their unanticipated deleterious effects on lysosomal function.

References and Notes

1. T. Braulke, J. S. Bonifacino, *Biochim. Biophys. Acta* **1793**, 605 (2009).
2. M. Bao, J. L. Booth, B. J. M. Elmendorf, W. M. Canfield, *J. Biol. Chem.* **271**, 31437 (1996).
3. S. Tiede *et al.*, *Nat. Med.* **11**, 1109 (2005).
4. M. Kudo *et al.*, *J. Biol. Chem.* **280**, 36141 (2005).
5. K. H. Paik *et al.*, *Hum. Mutat.* **26**, 308 (2005).
6. S. Kornfeld, W. S. Sly, in *The Metabolic and Molecular Bases of Inherited Disease*, C. R. Scriver *et al.*, Eds. (McGraw-Hill, New York, 2001), pp. 3421–3452.
7. M. Kudo, W. M. Canfield, *J. Biol. Chem.* **281**, 11761 (2006).
8. K. Kollmann *et al.*, *Eur. J. Cell Biol.* **89**, 117 (2010).
9. S. Pohl *et al.*, *J. Biol. Chem.* **285**, 23936 (2010).
10. A. Elagoz, S. Benjannet, A. Mammarbassi, L. Wickham, N. G. Seidah, *J. Biol. Chem.* **277**, 11265 (2002).
11. N. G. Seidah *et al.*, *Proc. Natl. Acad. Sci. U.S.A.* **96**, 1321 (1999).
12. J. Sakai, A. Nohturfft, J. L. Goldstein, M. S. Brown, *J. Biol. Chem.* **273**, 5785 (1998).
13. M. S. Brown, J. L. Goldstein, *Proc. Natl. Acad. Sci. U.S.A.* **96**, 11041 (1999).
14. J. M. Rojek, A. M. Lee, N. Nguyen, C. F. Spiropoulou, S. Kunz, *J. Virol.* **82**, 6045 (2008).
15. J. Stirling, P. O'Hare, *Mol. Biol. Cell* **17**, 413 (2006).
16. R. B. Rawson, D. Cheng, M. S. Brown, J. L. Goldstein, *J. Biol. Chem.* **273**, 28261 (1998).
17. J. Sakai *et al.*, *Mol. Cell* **2**, 505 (1998).
18. S. Müller-Loennies, G. Galliciotti, K. Kollmann, M. Glatzel, T. Braulke, *Am. J. Pathol.* **177**, 240 (2010).
19. K. Schlombs, T. Wagner, J. Scheel, *Proc. Natl. Acad. Sci. U.S.A.* **100**, 14024 (2003).
20. D. Patra *et al.*, *J. Cell Biol.* **179**, 687 (2007).
21. S. U. Walkley, M. T. Vanier, *Biochim. Biophys. Acta* **1793**, 726 (2009).
22. R. A. Saul, V. Proud, H. A. Taylor, J. G. Leroy, J. Spranger, *Am. J. Med. Genet. A* **135A**, 328 (2005).
23. N. G. Seidah, A. Prat, *J. Mol. Med.* **85**, 685 (2007).
24. J. L. Hawkins *et al.*, *J. Pharmacol. Exp. Ther.* **326**, 801 (2008).
25. J. M. Rojek *et al.*, *J. Virol.* **84**, 573 (2010).

Acknowledgments: We thank J. L. Goldstein for providing SRD-12B and CHO-7 cells. Lipoprotein-poor newborn calf serum and human LDL for selection of SRD-12B cells were provided by J. Heeren. We also thank J. Brand and C. Raithore for technical assistance. We are grateful to J. Bonifacino for critical reading of the manuscript and comments, and to K. Duncan for help in editing the manuscript. T. Braulke and S. Müller-Loennies hold a patent on the single-chain antibody fragment for the detection of M6P-containing proteins (International Patent no. PTC/EP2009/060224 and U.S./PTC Application no. 13/057,844). This work was supported by the Deutsche Forschungsgemeinschaft (SFB877/B3, GRK1459).

Supporting Online Material

www.sciencemag.org/cgi/content/full/333/6038/87/DC1
Materials and Methods
Figs. S1 to S5
References (*26*–*30*)

16 March 2011; accepted 20 May 2011
10.1126/science.1205677

Long Unfolded Linkers Facilitate Membrane Protein Import Through the Nuclear Pore Complex

Anne C. Meinema,[1]* Justyna K. Laba,[1]* Rizqiya A. Hapsari,[1]* Renee Otten,[1] Frans A. A. Mulder,[1] Annemarie Kralt,[2] Geert van den Bogaart,[1]† C. Patrick Lusk,[3] Bert Poolman,[1] Liesbeth M. Veenhoff[1,2]‡

Active nuclear import of soluble cargo involves transport factors that shuttle cargo through the nuclear pore complex (NPC) by binding to phenylalanine-glycine (FG) domains. How nuclear membrane proteins cross through the NPC to reach the inner membrane is presently unclear. We found that at least a 120-residue-long intrinsically disordered linker was required for the import of membrane proteins carrying a nuclear localization signal for the transport factor karyopherin-α. We propose an import mechanism for membrane proteins in which an unfolded linker slices through the NPC scaffold to enable binding between the transport factor and the FG domains in the center of the NPC.

The nuclear envelope (NE) consists of an inner (INM) and outer nuclear membrane (ONM) connected by the pore membrane at sites where the nuclear pore complexes (NPCs) are embedded. The ONM is continuous with the endoplasmic reticulum (ER). NPCs are composed of a membrane-anchored scaffold that stabilizes a cylindrical central channel, in which nucleoporins (Nups) with disordered phenylalanine-glycine (FG)–rich regions provide the selectivity barrier (*1*). For a membrane protein to move through the NPC, its transmembrane (TM) domains must pass through the pore membrane, while its extraluminal soluble domain(s) must pass through the NPC by a mechanism yet to be clarified (*2*–*4*). Some proteins reach the INM by diffusing through the pore membrane and adjacent lateral channels (*5*–*8*) and accumulate by binding nuclear structures (*9*, *10*). Other membrane proteins have a nuclear localization signal (NLS), and binding to transport factors karyopherin-α and karyopherin-β1 is required to pass the NPC and reach the INM (*11*, *12*). We sought to investigate the mechanism and path of nuclear transport of these integral INM proteins.

We first generated reporters using the *Saccharomyces cerevisiae* homolog of the human LEM domain–containing integral INM protein, Heh2. Heh2 is composed of a LEM domain, a bipartite NLS (hereafter h2NLS), a linker region (L), two TM segments flanking a luminal domain (LD), and a domain with homology to the C terminus of MAN1 (Fig. 1A) (*12*). The h2NLS is recognized by Kap60 (also known as Srp1 or Karyopherin-α), the yeast homolog of human Importin-α (*12*). Similar to Heh2, the reporter protein h2NLS-L-TM, consisting of green fluorescent protein (GFP) fused to amino acids 93 to 378 of Heh2, accumulated specifically at the NE (Fig. 1B). A control lacking the h2NLS, named L-TM, distributed over the NE and cortical ER. Although we could not resolve the INM from the ONM, we used the average pixel intensities at the NE and ER (NE-ER ratio) as a measure of INM accumulation (fig. S2, A and B). We validated this approach by confirming the localization of h2NLS-L-TM to the INM using immuno–electron microscopy (Fig. 1C and fig. S2C). h2NLS-L-TM accumulated 33-fold at the NE (Fig. 1B), whereas L-TM accumulated only 2-fold.

[1]Departments of Biochemistry and Biophysical Chemistry, Groningen Biomolecular Sciences and Biotechnology Institute, Netherlands Proteomics Centre, Zernike Institute for Advanced Materials, University of Groningen, Nijenborgh 4, 9747 AG, Groningen, Netherlands. [2]Department of Neuroscience, European Research Institute on the Biology of Ageing, University Medical Centre Groningen, Groningen, Netherlands. [3]Department of Cell Biology, Yale School of Medicine, New Haven, CT 06519, USA.

*These authors contributed equally to this work.
†Present address: Department of Neurobiology, Max Planck Institute for Biophysical Chemistry, Am Faßberg 11, 37077 Göttingen, Germany.
‡To whom correspondence should be addressed. E-mail: l.m.veenhoff@rug.nl

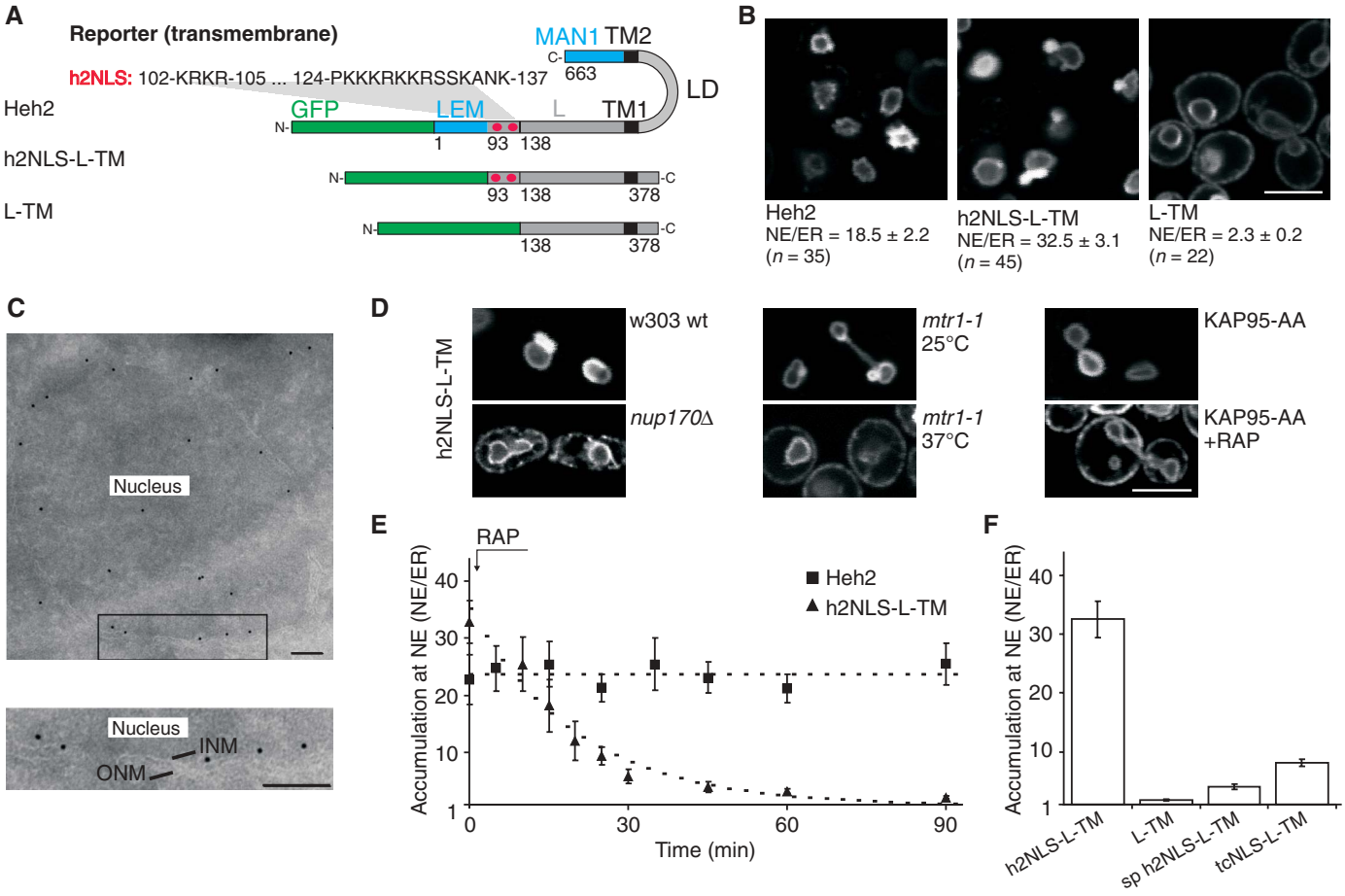

Fig. 1. The NLS-containing domain (h2NLS-L) of Heh2 is sufficient for accumulation at the INM. (**A**) Representation of Heh2-based GFP-fusion reporter proteins. (**B**) Confocal fluorescence images of yeast expressing the indicated proteins. Average NE/ER ratios are shown. (**C**) Immuno–electron micrograph of h2NLS-L-TM in the KAP95-AA strain labeled with antibodies against GFP and 10-nm-diameter gold-conjugated secondary antibody: 64% at the INM ($n = 350$, fig. S1D). (**D**) h2NLS-L-TM is mislocalized in a *Nup170*Δ strain (left), in a RanGEF mutant strain (*mtr1-1*) at nonpermissive temperature (middle), and in the KAP95-AA strain upon addition of rapamycin (RAP) (right). (**E**) The accumulation at the NE of h2NLS-L-TM (▲) and Heh2 (■) in the KAP95-AA strain as a function of time after anchoring of Kap95 (RAP at $t = 0$, $n \geq 13$). (**F**) The accumulation at the INM of reporter containing a bipartite h2NLS (h2NLS-L-TM), without NLS (L-TM), with single partite NLS (sp h2NLS-L-TM), or with tandem cNLS (tcNLS-L-TM) ($n \geq 32$). SEM is indicated; scale bars: (B and D) 5 μm and (C) 250 nm.

Transport of h2NLS-L-TM was dependent on the Ran gradient and Nup170, similar to full-length Heh2 (Fig. 1D) (*12*). To confirm that the import of our membrane reporter was Kap60/95-mediated, we examined the distribution of h2NLS-L-TM in a Kap95 (Karyopherin-β–Importin-β–Rsl1) "anchor away" strain (KAP95-AA) (*13*). Upon addition of rapamycin, Kap95-FRB was trapped at Pma1-FKBP in the plasma membrane and no longer available for nuclear transport (fig. S2, D to F). Indeed, the accumulation of h2NLS-L-TM at the NE was markedly reduced (+RAP, Fig. 1D). Moreover, INM-localized reporter proteins redistributed to the ONM and ER upon addition of rapamycin, and the nuclear accumulation dropped with a half-time of 14 ± 2.7 min (Fig. 1E). By contrast, the fluorescence intensity of Heh2 at the NE remained unaltered for >90 min. Thus, while Heh2 is bound to nuclear factors, h2NLS-L-TM is fully mobile within the NE-ER network.

The h2NLS is a high-affinity NLS compared to the classical NLS (fig. S3). To assess whether this high affinity is required for import of h2NLS-L-TM, we replaced the bipartite h2NLS with lower-affinity NLSs: either a single-partite version of the h2NLS that lacked the first KRKR basic region (sp h2NLS) or a tandem classical NLS (tcNLS). Both membrane reporters still accumulated at the INM, but the NE/ER ratios were lower (8.1 and 4.0, respectively) than for h2NLS-L-TM (Fig. 1F), indicating a correlation between the affinity of Kap60 for an NLS and the nuclear accumulation of membrane proteins.

We then examined how the L domain contributes to targeting. The amino acid composition of the L domain and the large Stokes radius (45 Å) of purified recombinant h2NLS-L suggest that it is unstructured (fig. S4, A to C). In addition, nuclear magnetic resonance (NMR) spectra of (unlabeled) h2NLS-L were typical of disordered proteins. The absence of stable secondary and tertiary structure was gauged from a lack of signal dispersion of the backbone amides for h2NLS-L in one-dimensional ^{1}H-NMR spectra (Fig. 2A, shaded area) and of the side-chain methyl signals in [^{1}H-^{13}C]-HSQC (heteronuclear single-quantum coherence) spectra (fig. S4D). To evaluate whether the sequence of the linker region contributed to targeting, we replaced the coding regions of the L domain in h2NLS-L-TM with two synthetic sequences, LR1 and LR2. These were generated randomly but had the same relative amino acid abundance as L. LR1 and LR2 are also predicted to be unfolded (fig. S4A). Both h2NLS-LR1-TM and h2NLS-LR2-TM were efficiently transported to the INM in a Kap-dependent manner (Fig. 2B). Systematic truncations of LR1 and LR2 and the original linker (L) resulted in three sets of reporters with variable linker lengths (see tables S2 and S3). The shortest truncations of each linker set did not accumulate at the nucleus (Fig. 2B). Indeed, we observed a marked dependence of INM import on linker length (Fig. 2C). Reporters with a synthetic TM segment and reporters with 1, or all 10 TM segments of an ER protein, Sec61, were also efficiently imported to the INM (Fig. 3). An "NLS-L-TM"-sorting signal could be recognized in Heh1 and, indeed, its NLS-linker-domain, even though lacking

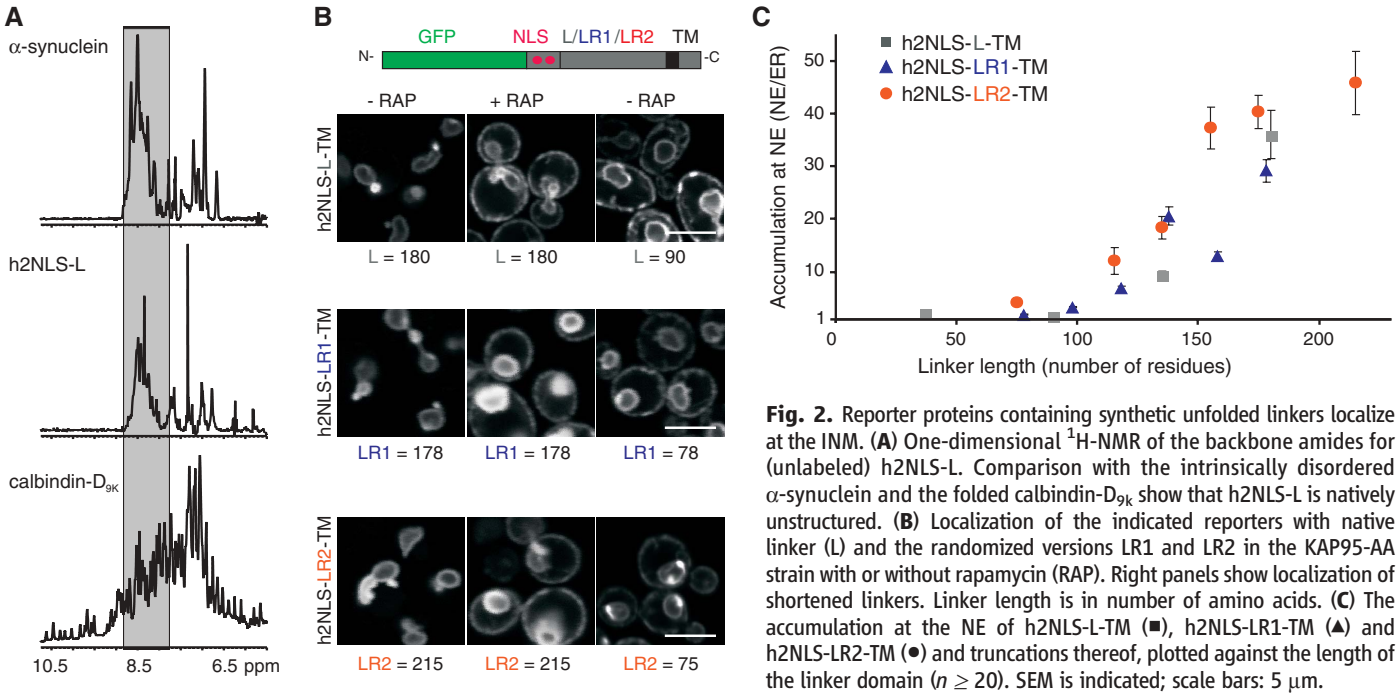

Fig. 2. Reporter proteins containing synthetic unfolded linkers localize at the INM. (**A**) One-dimensional ^{1}H-NMR of the backbone amides for (unlabeled) h2NLS-L. Comparison with the intrinsically disordered α-synuclein and the folded calbindin-D_{9k} show that h2NLS-L is natively unstructured. (**B**) Localization of the indicated reporters with native linker (L) and the randomized versions LR1 and LR2 in the KAP95-AA strain with or without rapamycin (RAP). Right panels show localization of shortened linkers. Linker length is in number of amino acids. (**C**) The accumulation at the NE of h2NLS-L-TM (■), h2NLS-LR1-TM (▲) and h2NLS-LR2-TM (●) and truncations thereof, plotted against the length of the linker domain ($n \geq 20$). SEM is indicated; scale bars: 5 μm.

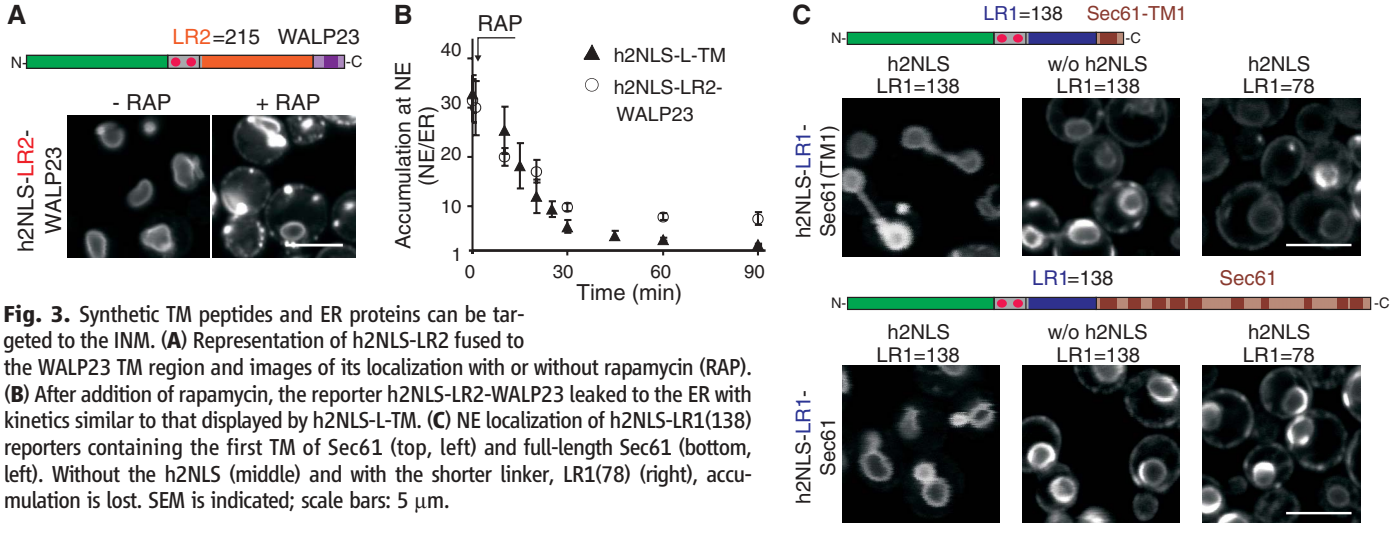

Fig. 3. Synthetic TM peptides and ER proteins can be targeted to the INM. (**A**) Representation of h2NLS-LR2 fused to the WALP23 TM region and images of its localization with or without rapamycin (RAP). (**B**) After addition of rapamycin, the reporter h2NLS-LR2-WALP23 leaked to the ER with kinetics similar to that displayed by h2NLS-L-TM. (**C**) NE localization of h2NLS-LR1(138) reporters containing the first TM of Sec61 (top, left) and full-length Sec61 (bottom, left). Without the h2NLS (middle) and with the shorter linker, LR1(78) (right), accumulation is lost. SEM is indicated; scale bars: 5 μm.

homology to that of Heh2, promoted INM targeting (fig. S5A).

Next, we determined whether the transport of the reporters across the NPC depends on specific FG regions of nucleoporins (*14*–*16*). A strain that lacks the GLFG repeats of Nups 100, 145, and 57 (*17*), which are anchored to both the cytoplasmic and nucleoplasmic halves of the NPC scaffold (*18*), showed 7.5-fold decreased NE accumulation (SWY2950, Fig. 4A). Minimal effects were seen with single deletions (fig. S5B) and in strains lacking the FG regions from the asymmetric localized Nups (SWY3062, SWY3042), whereas Kap60/95-mediated transport of soluble cargo (tcNLS-GFP) was affected in all three strains.

Our data point toward passage of the extraluminal soluble domains of the membrane proteins through the central channel, which is expected to place few constraints on the bulkiness of these domains. Indeed, membrane proteins with up to 174-kD soluble domains were imported to the INM, although the efficiency decreased with increasing size (Fig. 4B). To further support the suggestion that the extraluminal soluble domains pass through the central channel, we designed experiments to trap the reporters in transit through the NPC. We constructed a strain expressing FRB-tagged FG-Nup Nsp1. The C-terminal FRB tag on Nsp1 is anchored on the pore side of the scaffold of the NPC (*16*, *18*–*20*). A reporter containing FKBP at its N terminus was expressed to enable rapamycin-dependent trapping at Nsp1-FRB in the NPC (fig. S5C). Addition of rapamycin yielded a punctate stain typical of NPC-localized proteins; without rapamycin the reporter distributed evenly over the NE (Fig. 4C and fig. S5D). Next, we assessed whether trapping of the reporter at the NPC affected transport. We used a reporter expressed at higher levels (with an additional N-terminal protein A tag) and saw a blockage of INM import and steady increase in fluorescence at the ER from newly synthesized proteins, after rapamycin addition (Fig. 4D and fig. S5E). Trapping of the reporter specifically blocked transport of membrane proteins and not soluble proteins (fig. S5, F and G). Thus, the h2NLS-containing N terminus of the reporter passes where Nsp1 is anchored to the NPC scaffold and within the central channel of the NPC.

Here we have elucidated the NLS-dependent mechanism of membrane protein transport through

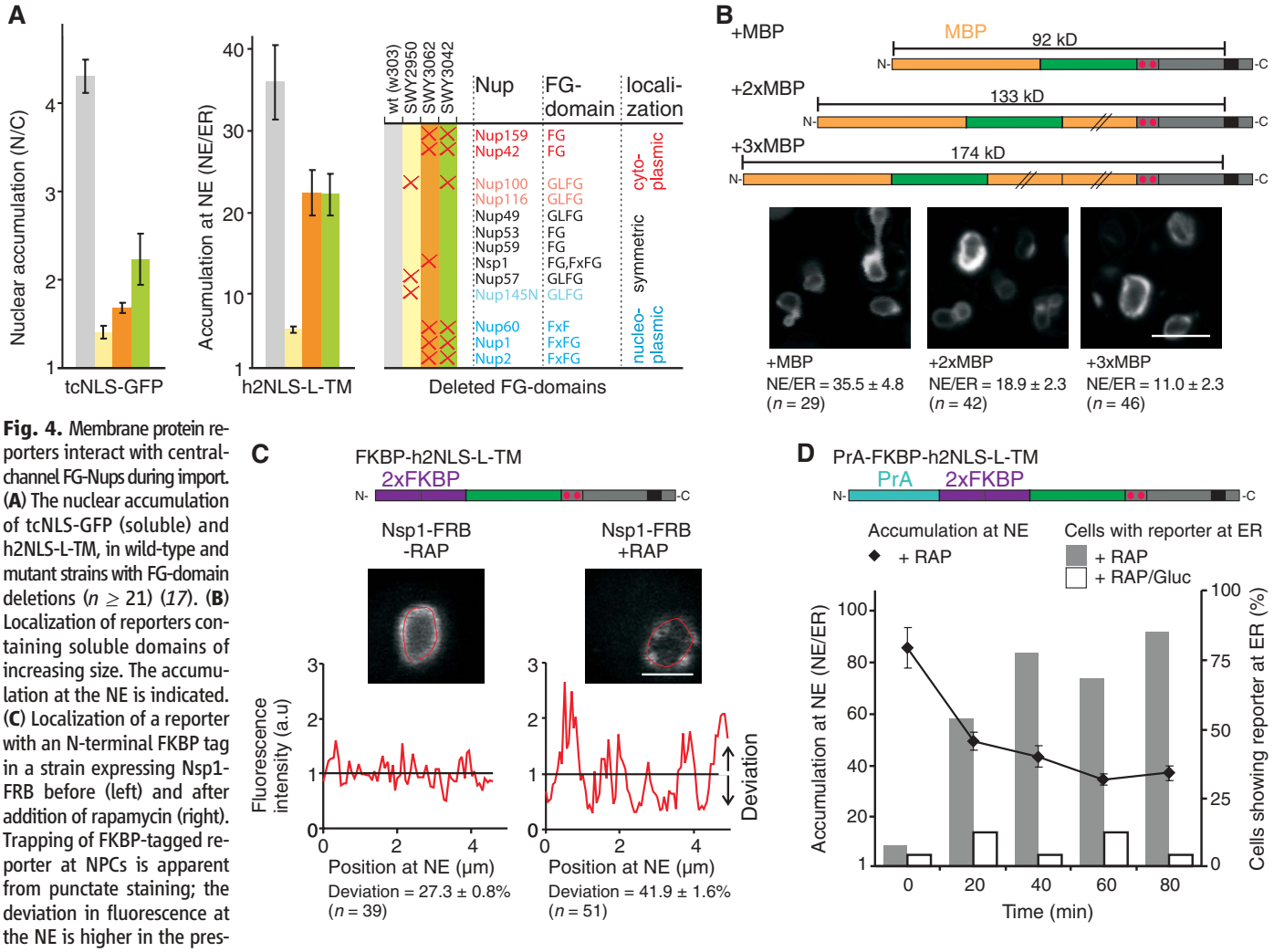

Fig. 4. Membrane protein reporters interact with central-channel FG-Nups during import. (**A**) The nuclear accumulation of tcNLS-GFP (soluble) and h2NLS-L-TM, in wild-type and mutant strains with FG-domain deletions ($n \geq 21$) (*17*). (**B**) Localization of reporters containing soluble domains of increasing size. The accumulation at the NE is indicated. (**C**) Localization of a reporter with an N-terminal FKBP tag in a strain expressing Nsp1-FRB before (left) and after addition of rapamycin (right). Trapping of FKBP-tagged reporter at NPCs is apparent from punctate staining; the deviation in fluorescence at the NE is higher in the presence of rapamycin. (**D**) Rapamycin-dependent trapping of PrA-FKBP–tagged reporter at Nsp1-FRB blocked import as observed from increased ER-localized reporter. Percentage of cells showing fluorescence at the ER ($n \geq 100$, bars) and the average NE/ER ratio ($n \geq 13$, symbols) upon addition of rapamycin (RAP, filled bars and ◆) or glucose (inhibition of reporter synthesis) and rapamycin (RAP/Gluc, open bars). SEM is indicated; scale bars: (B) 5 μm and (C) 2 μm.

the NPC. The Heh2-derived reporter proteins accumulate at the INM, not because they are retained or trapped at the INM, but because Kap60/95-mediated import is faster than export. The signal for targeting to the INM is composed of a natively unfolded linker that spaces the TM segment and a high-affinity NLS. It takes little energy to stretch the linker to allow the NLS, with bound karyopherins, to dodge between the NPC scaffold and the karyopherins to bind the FG-Nups (fig. S6). The proposed transport route implies that, at least transiently, openings must exist between the space immediately aligning the pore membrane and the central channel. At present, structures of the NPC lack the resolution to reveal such conduits, but its plasticity and the overall lattice-like scaffold structure observed in electron microscopy (*8*, *21*, *22*) and computational structures (*18*) are compatible with our model. The transport mechanism described here is likely to exist in parallel with a previously proposed route based on diffusion and nuclear retention (*2*, *5*–*7*, *9*, *10*).

References and Notes

1. S. R. Wente, M. P. Rout, *Cold Spring Harb. Perspect. Biol.* **2**, a000562 (2010).
2. N. Zuleger, N. Korfali, E. C. Schirmer, *Biochem. Soc. Trans.* **36**, 1373 (2008).
3. C. P. Lusk, G. Blobel, M. C. King, *Nat. Rev. Mol. Cell Biol.* **8**, 414 (2007).
4. T. Ohba, E. C. Schirmer, T. Nishimoto, L. Gerace, *J. Cell Biol.* **167**, 1051 (2004).
5. P. Malik *et al.*, *Cell. Mol. Life Sci.* **67**, 1353 (2010).
6. B. Soullam, H. J. Worman, *J. Cell Biol.* **130**, 15 (1995).
7. W. Wu, F. Lin, H. J. Worman, *J. Cell Sci.* **115**, 1361 (2002).
8. J. E. Hinshaw, B. O. Carragher, R. A. Milligan, *Cell* **69**, 1133 (1992).
9. J. Ellenberg *et al.*, *J. Cell Biol.* **138**, 1193 (1997).
10. C. Ostlund, J. Ellenberg, E. Hallberg, J. Lippincott-Schwartz, H. J. Worman, *J. Cell Sci.* **112**, 1709 (1999).
11. Y. Turgay *et al.*, *EMBO J.* **29**, 2262 (2010).
12. M. C. King, C. P. Lusk, G. Blobel, *Nature* **442**, 1003 (2006).
13. H. Haruki, J. Nishikawa, U. K. Laemmli, *Mol. Cell* **31**, 925 (2008).
14. S. Frey, R. P. Richter, D. Görlich, *Science* **314**, 815 (2006).
15. R. Peters, *Bioessays* **31**, 466 (2009).
16. M. P. Rout *et al.*, *J. Cell Biol.* **148**, 635 (2000).
17. L. A. Strawn, T. Shen, N. Shulga, D. S. Goldfarb, S. R. Wente, *Nat. Cell Biol.* **6**, 197 (2004).
18. F. Alber *et al.*, *Nature* **450**, 695 (2007).
19. N. Schrader *et al.*, *Mol. Cell* **29**, 46 (2008).
20. S. M. Bailer, C. Balduf, E. Hurt, *Mol. Cell. Biol.* **21**, 7944 (2001).
21. D. Frenkiel-Krispin, B. Maco, U. Aebi, O. Medalia, *J. Mol. Biol.* **395**, 578 (2010).
22. Q. Yang, M. P. Rout, C. W. Akey, *Mol. Cell* **1**, 223 (1998).

Acknowledgments: We thank M. C. King, M. P. Rout, and D. J. Slotboom for discussion; V. Krasnikov for help with confocal microscopy; and M. Graham for assistance with immunoelectron microscopy. We thank S. R. Wente, U. K. Laemmli, and M. P. Rout for reagents and strains. This work was supported by funding from the Netherlands Organization for Scientific Research (VIDI fellowship to L.M.V. and F.A.A.M.; Top-subsidy grant 700.56.302 to B.P.). L.M.V. conceived the project. Experiments were performed and analyzed by A.C.M., J.K.L., R.A.H., C.P.L., and A.K. NMR was performed by R.O. and F.A.A.M. G.v.d.B. helped with image analysis. Experiments were designed and the manuscript was written by A.C.M., C.P.L., B.P., and L.M.V.

Supporting Online Material

www.sciencemag.org/cgi/content/full/science.1205741/DC1
Materials and Methods
Figs. S1 to S6
Tables S1 to S3
References

17 March 2011; accepted 10 May 2011
Published online 9 June 2011;
10.1126/science.1205741